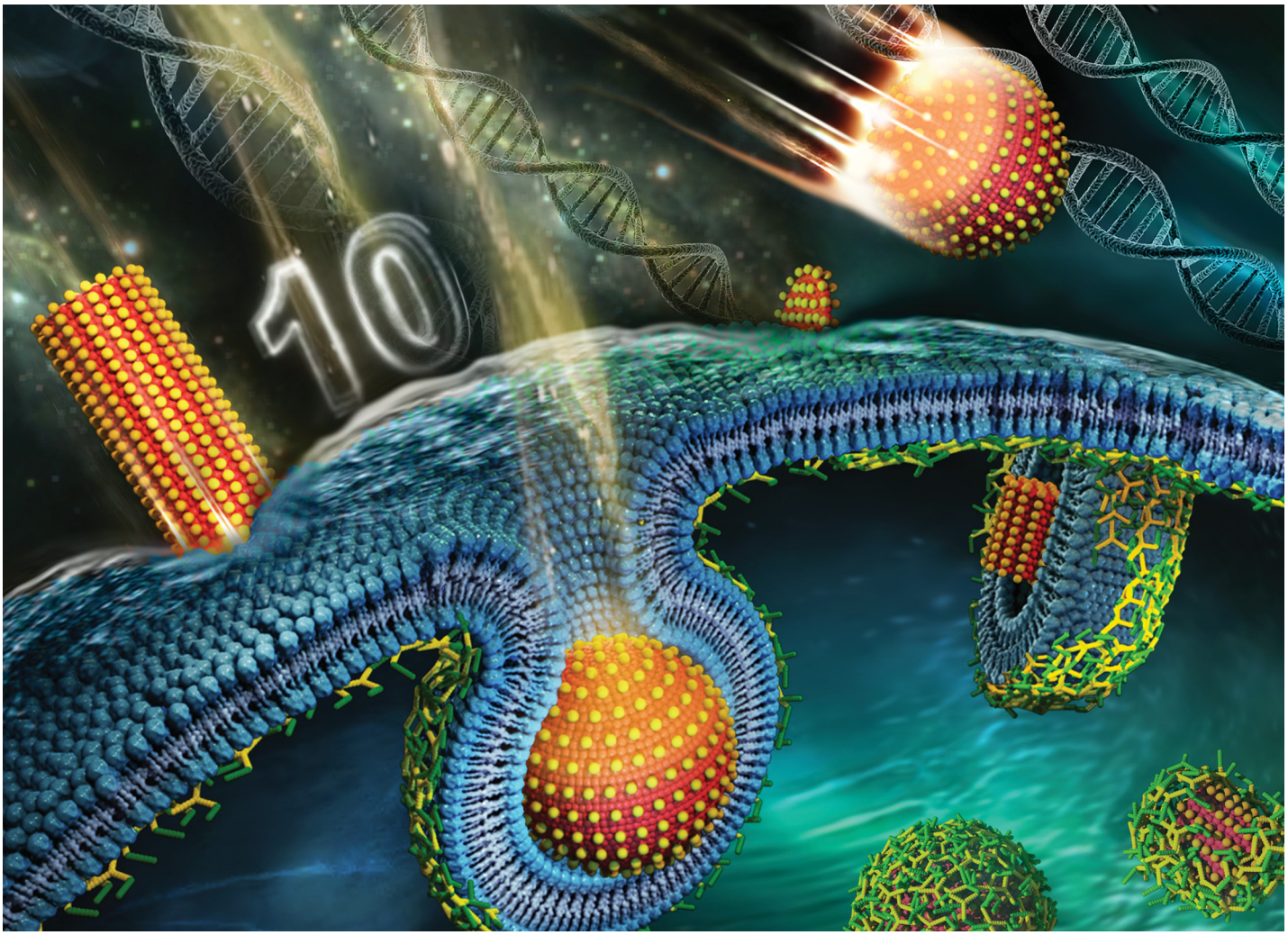

Showcasing a study on the influence of nanoparticle shape by clathrin-mediated endocytosis by Dr Ye Li *et al.* at Beijing Forestry University.

A computational study of the influence of nanoparticle shape on clathrin-mediated endocytosis

Clathrin-mediated endocytosis is shape sensitive for nanoparticle. Understanding the dynamics mechanism of clathrin-mediated endocytosis of nanoparticle will help to design targeted nanomedicines with an improved efficacy.

As featured in:

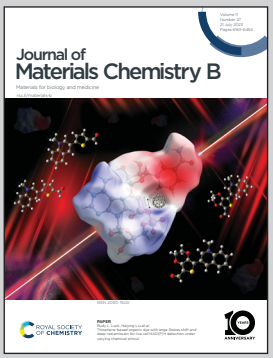

See Ye Li *et al.*, *J. Mater. Chem. B*, 2023, **11**, 6319.

ROYAL SOCIETY OF CHEMISTRY

rsc.li/materials-b

Registered charity number: 207890

Journal of Materials Chemistry B

ROYAL SOCIETY OF CHEMISTRY

PAPER

View Article Online
View Journal | View Issue

Cite this: J. Mater. Chem. B, 2023, 11, 6319

A computational study of the influence of nanoparticle shape on clathrin-mediated endocytosis†

Ye Li, *[abc] Man Zhang,[abc] Yezhuo Zhang,[abc] Xinhui Niu,[abc] Zhendan Liu,[abc] Tongtao Yue[d] and Wen Zhang[abc]

Nanoparticles have been widely used in biomedical applications such as gene/drug delivery, molecular imaging and diagnostics. Among the physicochemical properties, shape is a vital design parameter for tuning the cell uptake of nanoparticles. However, the regulatory mechanism remains elusive due to the complexity of the cell membrane and multiple pathways of cell uptake. Therefore, in this computational study, we design and clarify cell membrane wrapping on different shaped nanoparticles (sphere, rod and disk) with a clathrin assembly to model the clathrin-mediated endocytosis, which is an important pathway of nanoparticle cell uptake. Our simulations revealed that the clathrin-mediated endocytosis is shape sensitive for nanoparticles. Spherical nanoparticles are easier to be wrapped by the membrane with the self-assembly of clathrins than the other shaped nanoparticles with the same volume, and the efficiency declines with the increase in the nanoparticle shape anisotropy. Furthermore, simulation results showed clear evidence that rotation is one of the typical characteristics determining the kinetics of clathrin-mediated endocytosis of shaped nanoparticles. Especially for rod nanoparticles with high aspect ratios, nanoparticle rotation occurs in both the invagination and wrapping stages, which is different from the case without clathrins. The size and shape mismatch between the clathrin-mediated vesicle and the nanoparticle determines how the nanoparticle rotates and is wrapped by the membrane. In addition, the wrapping time of nanoparticles depends not only on the shape of the nanoparticle but also on its initial orientation and size, the rate of clathrin self-assembly and the surface tension of the membrane. These results provide insights into the interplay between cell membrane wrapping and clathrin assembly, where the nanoparticle shape matters. Understanding the dynamics mechanism of clathrin-mediated endocytosis of nanoparticles will help to design targeted nanomedicines with an improved efficacy.

Received 15th February 2023,
Accepted 9th May 2023

DOI: 10.1039/d3tb00322a

rsc.li/materials-b

1. Introduction

With the development of nanotechnology, nanoparticles (NPs) have opened new avenues for various biomedical applications such as drug/gene delivery,[1,2] molecular imaging[3,4] and diagnostic purposes.[5–7] The process of NP internalization into the cell is very important in most of the biomedical applications. Clathrin-mediated endocytosis (CME) is one of the major internalization pathways for eukaryotic cells. In previous work, it has been reported that the uptake of numerous types of NPs is by CME.[8–11] Therefore, a better understanding of how the clathrin mediates nanoparticle (NP) endocytosis is essential for the design of NPs as drug/gene delivery carriers.

In previous work, numerous results have indicated that the physicochemical properties of NPs[12] such as size,[13–18] shape,[19–25] stiffness[26–30] and surface property[31–34] can affect their internalization pathway and efficiency. In particular, experimental studies demonstrated that CME is size-dependent internalization of NPs.[35] Using both microscopic imaging and biological techniques to explore the processes of LDH nanoparticles, it was also found that NPs of size ranging from 50 nm

[a] State Key Laboratory of Tree Genetics and Breeding, College of Biological Sciences and Technology, Beijing Forestry University, Beijing 100083, China. E-mail: liye0223@bjfu.edu.cn
[b] Key Laboratory of Genetics and Breeding in Forest Trees and Ornamental Plants, Ministry of Education, College of Biological Sciences and Technology, Beijing Forestry University, Beijing 100083, China
[c] The Tree and Ornamental Plant Breeding and Biotechnology Laboratory of National Forestry and Grassland Administration, College of Biological Sciences and Technology, Beijing Forestry University, Beijing 10083, China
[d] Institute of Coastal Environmental Pollution Control, Key Laboratory of Marine Environment and Ecology, Ministry of Education, Ocean University of China, Qingdao 266100, China

† Electronic supplementary information (ESI) available. See DOI: https://doi.org/10.1039/d3tb00322a

to 200 nm were selectively internalized into cells through CME.[36] To analyze the selectivity mechanism for NP size underlying CME, in our previous computational study, we found that the clathrin assemblage has a certain range of sizes, which ensures whether membrane wrapping on different size of NPs is promoted or suppressed.[14] Besides, it was demonstrated that the interaction between the membrane and NP can be influenced by clathrin-coated pits.[37] In addition, Deng *et al.* have demonstrated that the NP size, ligand density and membrane stiffness can influence the internalization of NPs by CME, and that the intermediate NP size and ligand density favor NP endocytosis.[38] Moreover, surface modification also plays a great role in NP internalization, which can be tuned to alter its cell uptake mechanism and subcellular trafficking. It has been revealed that positively charged NPs internalize rapidly *via* the CME pathway.[39,40] Besides, it was observed that cationic nanoprobes electrostatically interact with the cell membrane and enter into the cell *via* CME.[41] The uptake of decorated NPs used for drug delivery to cancer cells has also been revealed by CME.[42–44] Compared with different elastic NPs, the soft NPs are less efficient to be fully wrapped by the lipid membrane due to their elastic deformation and high local curvature.[45] Besides, the NP shape plays a vital role in the interaction of NP-membrane[45] and affects the internalization pathways.[46] For nanodrug delivery systems, the shape of NPs greatly affects cell internalization as well as tumor tissue penetration.[47] The endocytosis efficiency is higher for spherocylindrical NPs than for spheres by receptor-mediated endocytosis.[23] Besides, it was demonstrated that ellipsoids with intermediate aspect ratios show easier endocytosis than that of NPs with low and high aspect ratios.[48] However, the penetrating capability of NPs with sharp edges has obvious advantages.[49] Therefore, a fundamental question arises regarding how the shape of NPs regulate cell uptake by CME. This is now generally unclear but of great significance.

The cell membrane consists of lipid molecules and membrane proteins, which provide an important platform for the exchange of the matter between the cytoplasm and the external medium. CME occurs with the assembly of clathrins, which is the major pathway for NP internalization. In recent years, molecular simulation has become a significant complementary method to experiments. A lot of theoretical and computational models have investigated the mechanism of receptor-mediated endocytosis of NPs.[45,50,51] Besides, the composition of lipid membrane is very important for the interaction between the NP and the membrane. It is demonstrated that the membrane binding of cationic lipid NPs is an entropy-driven process.[52] However, a common assumption of these models is that the membrane wrapping around NPs is solely accomplished by a lipid bilayer, while the roles of clathrin coat and assembly were not considered explicitly. Besides, the shape of NPs can influence its internalization efficiency, but majority of previous studies focused on spherical NPs.[14] Considering the critical roles of clathrins in the endocytosis of NP, here we studied the cellular uptake of different shaped NPs with a focus on the clathrin assembly by dissipative particle dynamics (DPD) simulation. Besides, the coordinate relationship between the rotations of different shaped NPs, the assembly of clathrins and the binding of ligand–receptor during endocytosis were systematically investigated. This work will underpin the design of new strategies for drug/gene delivery into cells using NPs.

2. Computational details

2.1. Coarse-grained models

To simulate the CME of different shaped NPs, four different shapes of NPs with the same volume and same ligand density, namely, sphere-shaped NPs (diameter of 7.1 nm, D = 7.1 nm), long rod-shaped NPs (diameter of 4.5 nm and height of 9.7 nm, D = 4.5 nm and H = 9.7 nm), short rod-shaped NPs (D = 5.8 nm and H = 5.8 nm) and disk-shaped NPs (D = 9.7 nm and H = 1.9 nm) were designed in our work (Fig. S1A, ESI†). All different shaped NPs are composed of hydrophilic beads (denoted as P), which are constrained to move as a rigid body (Fig. S1A, ESI†). The ligands (denoted as L) coated onto the surface of NP are modeled as single solid beads (Fig. S1A, ESI†), which have attraction with the receptors on the lipid membrane. For the lipid membrane, the head group of three hydrophilic beads (denoted as H) to connect to two hydrophobic tails of equal length with five hydrophobic beads (denoted as T) represents the lipid molecule (Fig. S1B, ESI†), which can show the typical phase behaviors of the lipid membrane.[53,54] In CME, clathrins and AP2 adaptor protein complex are two main proteins that participate in the endocytosis process.[55] AP2 intermediates bring the cargo and clathrin together.[56] The plasma membrane-specific lipid phosphatidylinositol-4,5-bisphosphate (PtdIns(4,5)P_2) binds AP2 and clathrins. To simplify by following the principle, the role of AP2 is replaced by the attractive interaction between the membrane and clathrin. The receptor represents the role of PtdIns(4,5)P_2 to link the NP and clathrin (Fig. S1C, denoted as R, ESI†), which has the similar structure to lipid and has been used in our previous work.[14] Note that the real clathrin triskelion is composed of three heavy chains. The three heavy chains provide the structural backbone, and the three light chains are thought to regulate the formation and disassembly of a clathrin lattice. To simulate the structure and function of the clathrin, the clathrin model (Fig. S1D, denoted as C, ESI†) has three heavy chains (denoted as C_H) of 7 beads with the equal length, and each connects a single light chain of 5 beads (denoted as C_L), which was obtained from electron cryomicroscopy.[57] The three short light chains (C_L) are radiating from the center of the clathrin, which is shown in green on the clathrin model (Fig. S1D, ESI†). In addition, the three longer heavy chains (C_H) associate with the short light chains, being connected through a corner, which is shown in yellow on the clathrin model (Fig. S1D, ESI†). To simulate the self-assembly process of clathrins on the membrane, the detail of the interaction parameters are described in the following sections. In our simulations, the clathrin is simplified as a rigid body, and the effect of intrinsic protein deformation is disregarded, which has been used in our previous work.[14] Thus, the initial configuration is composed of lipid molecules, receptors, clathrins that are put close to the distal

monolayer of the membrane and in the cytoplasm, and NP which is placed above the membrane (Fig. S1E, ESI†). Coarse grained single beads represent solution molecules (denoted as *W*), which were included explicitly in our simulation system. The simulation box size is 38.8 nm × 38.8 nm × 32.3 nm. We show the initial configuration of the system from the side view in Fig. S1E (ESI†) and bottom view in Fig. S1F (ESI†).

2.2. Dissipative particle dynamics simulation

In this work, DPD simulations were performed to study the endocytosis of different shaped NPs by CME. DPD was introduced for the first time to study the hydrodynamics of complex fluids, and has been widely used in biomembrane systems, especially the NP-membrane interaction, which is a coarse-grained simulation with hydrodynamic interaction.[23,49,58–61] In DPD, the dynamics of the elementary units are soft beads that are governed by Newton's equation of motion, $dr_i/dt = v_i$ and $dv_i/dt = f_i/m_i$. Typically, three forces exerted on bead i by bead j are composed of conservative force F_{ij}^{C}, dissipative force F_{ij}^{D}, and random force F_{ij}^{R}. The total force exerted on bead i was determined as follows:

$$F_i = \sum_{i \neq j} \left(F_{ij}^{C} + F_{ij}^{D} + F_{ij}^{R} \right) \quad (1)$$

The conservative force between beads i and j has the following form:

$$F_{ij}^{C} = a_{ij} \hat{\mathbf{r}}_{ij} \max\left\{ 1 - {r_{ij}}/{r_c}, 0 \right\} \quad (2)$$

where a_{ij} (in $k_B T/r_c$) is the maximum repulsive force constant between beads i and j, $\mathbf{r}_{ij} = \mathbf{r}_j - \mathbf{r}_i$ (the distance between beads i and j), $r_{ij} = |\mathbf{r}_{ij}|$, $\hat{\mathbf{r}}_{ij} = \mathbf{r}_{ij}/|\mathbf{r}_{ij}|$, and r_c is the cutoff radius of the force.

To reproduce the process of CME of different shaped NPs, the interaction parameters between beads of the same type were set to $a_{WW} = a_{HH} = a_{TT} = 25$, $a_{C_H H_H} = 35$, $a_{C_L C_L} = 15$ and those between the different types of beads were $a_{TW} = 80$, $a_{HT} = a_{CT} = 50$, $a_{CH} = a_{CR} = 15$, $a_{C_L C_H} = 10$ and $a_{HW} = a_{CW} = 25$. All the interaction parameters in this system are shown in Table S1 (ESI†), referring from our previous simulation studies.[14,62] If the interaction parameter is smaller than 25 (the water–water interaction parameter), the interaction can be effectively regarded as attractive. Otherwise, the interaction is repulsive if the parameter is larger than 25.[63,64]

The dissipative force is expressed as follows:

$$F_{ij}^{D} = -\gamma (1 - r_{ij}/r_c)^2 (\hat{r}_{ij} \cdot v_{ij}) \hat{r}_{ij} \quad (3)$$

where γ is the friction coefficient, and $v_{ij} = v_i - v_j$ (the relative velocity between beads i and j).

The random force is given as follows:

$$F_{ij}^{R} = \sigma (1 - r_{ij}/r_c) \theta_{ij} \hat{r}_{ij} \quad (4)$$

where σ is the noise amplitude and θ_{ij} represents an uncorrelated random variable with zero mean and unit variance.

For each lipid molecule, the interaction between neighboring beads within the same molecule is described by a harmonic spring force:

$$F_S = K_S (r_{ij} - r_{eq}) \hat{r}_{ij} \quad (5)$$

where the spring constant $K_S = 128$ and the equilibrium bond length $r_{eq} = 0.7$.

To maintain the bending rigidity of lipids, the force constraining the variation of bond angle is taken as follows:

$$F_\varphi = -\nabla U_\varphi \text{ and } U_\phi = K_\phi (1 - \cos(\phi - \phi_0)) \quad (6)$$

where ϕ is the bond angle, which is defined by the scalar product of two bonds respectively connecting beads $i-1$, i, and i, $i+1$.[65] The equilibrium bond angle $\phi_0 = \pi$ and $K_\phi = 10.0$ is the bond bending constant.

In this work, all simulations were performed in the *NVT* ensembles. Besides, periodic boundary conditions were implemented in all the three directions. The system was evolved using the velocity-Verlet algorithm with a time step of $\Delta t = 0.02$.[66]

To represent the membrane responses for CME, we used a particular variant of the DPD method (N-varied DPD).[67] In this technique, to keep surface tension of the lipid membrane, we adjusted the lipid number per area (LNPA) in the boundary region of the membrane, which plays a role as a reservoir of lipids. The value of LNPA in the boundary region (denoted as ρ_{LNPA}) is kept within a defined range ($\rho_{LNPA}^{min} < \rho_{LNPA} < \rho_{LNPA}^{max}$) by addition/deletion moves of lipids. If the local lipid area density is less than ρ_{LNPA}^{min}, new lipid molecules are inserted into the boundary region. Conversely, if the average area density of lipids in the boundary region exceeds ρ_{LNPA}^{max}, a corresponding number of lipids are deleted randomly from the boundary region. Simultaneously, a corresponding number of water beads are randomly deleted or added to keep the whole density of beads in the simulation box constant. Furthermore, in order to allow enough time to propagate the membrane tension to the whole membrane, we performed one addition/deletion move every 1500 time steps. In this work, the values of ρ_{LNPA}^{min} and ρ_{LNPA}^{max} were set to be 1.66 and 1.68, respectively, which make the value of ρ_{LNPA} fluctuating around 1.67. The value of $\rho_{LNPA} = 1.47$ represents the zero tension.[62] In the real biological processes, the negative membrane tension can be imposed by the cytoskeleton or dynamin to realize the endocytosis process.[68] To simulate the negative membrane tension, unless specified, we set the surface tension of membrane as $\rho_{LNPA} = 1.67$ to represent a negative surface tension in this study.

3. Results and discussion

3.1. Endocytosis dynamics processes for various shaped NPs with the clathrin self-assembly

Shape design is an important factor for NPs as drug/gene delivery carriers. To systematically reveal the effect of NP shape on the CME, four types of NPs with different shapes, which are long rod-shaped NPs with a diameter of 4.5 nm and height of 9.7 nm (D = 4.5 nm, H = 9.7 nm), short rod-shaped NPs

(D = 5.8 nm, H = 5.8 nm), disk-shaped NPs (D = 9.7 nm, H = 1.9 nm) and sphere-shaped NPs (D = 7.1 nm), that have the same volume and density of ligands were modeled (Fig. S1, ESI†). The effect of the initial angles between the normal direction of NPs and the horizontal direction of the lipid membrane, ϕ_0, was also studied. To investigate the process of the CME, in the initial state, NP was put above the membrane and 81 clathrin molecules were positioned at the opposite membrane side (Fig. S1, ESI†). We performed more than 5 parallel simulations. The final results are repeatable, but the intermediate processes may be lengthened for different parallel simulations. The typical results are shown in the following sections.

3.1.1. Clathrin-mediated endocytosis of long rod-shaped NPs. First, we simulated the endocytosis of long rod-shaped NPs and five initial NP orientations, including $\phi_0 = 0^\circ$, 30°, 45°, 60°, and 90°, were considered respectively. After simulation of 15 μs, the final snapshots of the CME at different initial angles of long rod-shaped NPs are shown in Fig. 1. The simulation results showed that long rod-shaped NPs of different initial orientations can be wrapped by the lipid membrane with the self-assembly of clathrins, but they have different endocytosis rates. The whole internalization processes can be roughly divided into two stages: the invagination stage (Fig. 1B) and the wrapping stage (Fig. 1C). In the invagination stage, under the binding of ligand–receptor, long rod-shaped NPs of different initial orientations rotated themselves to lie flat on the membrane (Fig. 1D). It was found that the initial orientation of NPs influences their invagination process (Fig. 1B). The results indicated that the most appropriate invagination angle for long rod-shaped NP is 45° (Fig. 1B), which is different from the favorable invagination angle of long rod-shaped NPs on the pure membrane. This result is very interesting but a counter-intuitive phenomenon. Usually, the long rod-shaped NP with an initial angle of 0° is favorable for receptor–ligand binding. In our previous studies, we have found that $\phi_0 = 0^\circ$ of long rod-shaped NPs in the invagination stage completes within the shortest simulation time.[20] We speculated that the initial self-assembly of clathrins can affect the stiffness of the membrane, which is not beneficial for the further invagination of long rod-shaped NPs with $\phi_0 = 0^\circ$.

In the wrapping stage, the obvious rotation of long rod-shaped NPs was also observed in CME, which is different from the endocytosis of long rod-shaped NPs without clathrins. In previous studies, they have revealed that usually different initial angles of long rod-shaped NPs rotated themselves to lie flat on the membrane,[69,70] and gradually wrapped by the pure lipid membrane with the same orientation.[22] However, in CME, the long rod-shaped NP has the second rotation in the wrapping stage. We speculated that the NP needs to rotate itself to promote clathrin rearrangement and realize further subsidence. Moreover, the self-assembly of clathrins tends to form an isotropic spherical cage structure. However, the wrapping of long rod-shaped NP is likely to form an asymmetric vesicle.

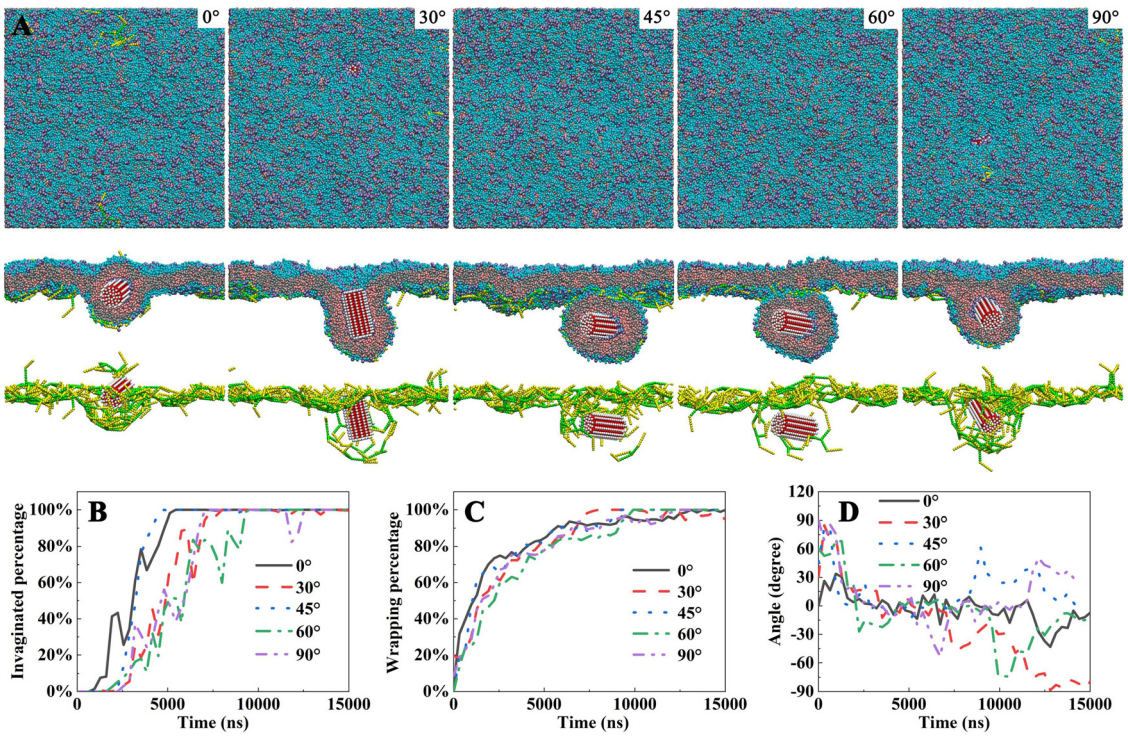

Fig. 1 Clathrin-mediated endocytosis of long rod-shaped NP (D = 4.5 nm and H = 9.7 nm) with different initial angles. (A) Final snapshots for clathrin-mediated endocytosis of different initial angles of long rod-shaped NPs from top, cross-sectional views, and only clathrin and NP. (B) Invaginated percentage evolution for long rod-shaped NPs. (C) Wrapping percentage evolution for long rod-shaped NPs. (D) Evolution of long rod-shaped NP orientation angles. In the figure, five initial orientations were compared.

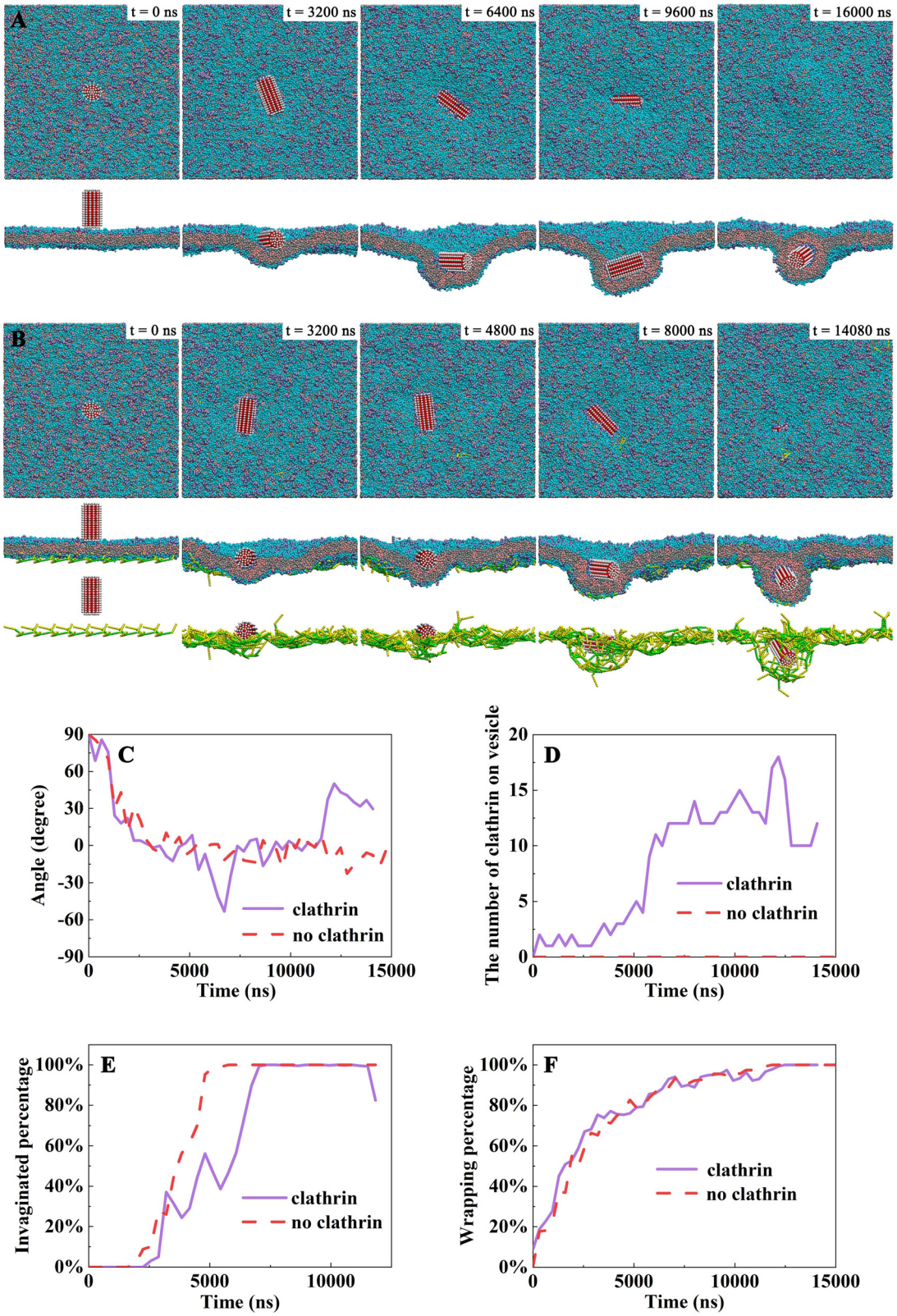

Fig. 2 Endocytosis kinetics for long rod-shaped NP with the initial orientation angle of 90°. Several typical snapshots during endocytosis of long rod-shaped NP in the absence of clathrin (A) and in the presence of clathrin (B). (C) Time evolutions of NP orientation angles. (D) Time evolutions of the clathrin number on vesicles. (E)linvaginated percentage of NPs as a function of time. (F) Wrapping percentage of NPs as a function of time.

The shape cooperation and adaption between the wrapping of NP and the clathrin self-assembly lead to further rotation of long rod-shaped NPs in the wrapping stage. Finally, long rod-shaped NPs tended to be wrapped by the membrane with a tilting angle (Fig. 1D). In addition, the final orientations of long rod-shaped NPs are not uniform, which should be entropy induced and affected by the self-assembly of clathrins (Fig. 1A and D). Besides, during CME, three typical endocytosis states were observed: first, NPs embedded into the membrane and "below" the membrane, but not complete engulfment (Fig. 1A, ϕ_0 = 30°), which is a metastable stable. Second, the NP was wrapped by the membrane and in the center of the membrane (Fig. 1A, ϕ_0 = 0°). Third, NP was completely wrapped by the membrane and "detached" from the planar membrane (Fig. 1A, ϕ_0 = 45°, 60°, and 95°).

To further investigate the role of clathrin assembly in membrane wrapping on long rod-shaped NPs, the typical snapshots of the endocytosis of long rod-shaped NPs (ϕ_0 = 90°) without and with clathrins are shown in Fig. 2A and B. Rotation is one of the vital characteristics for the endocytosis of long rod-shaped NPs (Fig. 2C). Compared without clathrins, the subsidence process of NPs became slow with the clathrin (Fig. 2E). This is because the initial self-assembly of clathrins rigidifies the local membrane patch, when the clathrin-mediated cage structure is not formed. In the wrapping stage, compared with the absence of clathrins, an obvious NP rotation was also found in the presence of clathrins (Fig. 2C). During the ligand–receptor binding, clathrin molecules were recruited by the local membrane curvature at the wrapping site (Fig. 2D), finally long rod-shaped NP completed endocytosis (Fig. 2B and F). Besides, the self-assembly of clathrins form the ellipsoid-shaped cage on the lower side of the membrane (Fig. 2B).

3.1.2. Clathrin-mediated endocytosis of short rod-shaped NPs. In order to further investigate the mechanism of CME for shape anisotropy NPs, we reduced the aspect ratio of NPs and studied the internalization of short rod-shaped NPs. The final snapshots of the CME at different initial angles of short rod-shaped NPs were shown in Fig. 3A. Rotation also plays an important role in the invagination of short rod-shaped NPs. In the invagination stage, short rod-shaped NPs with different initial angles rotated themselves to lie flat on the membrane (Fig. 3D), which is caused by the ligand–receptor interaction. However, compared with the absence of clathrins, the invagination percentage change tendency for NPs with different initial orientations is more complex in the presence of clathrins, which is determined by cooperative relationship between NP rotation and clathrin aggregation. With weak shape anisotropy, the short rod-shaped NP has no obvious rotation in the wrapping stage, which further confirms our speculation that the shape mismatch between the clathrin-mediated cage and the shape anisotropy of NPs can mediate NP rotation. Finally, the wrapping dynamic process of different initial orientations of short rod-shaped NPs has no obvious difference (Fig. 3C), after the lying down of NPs in the invagination process (Fig. 3B).

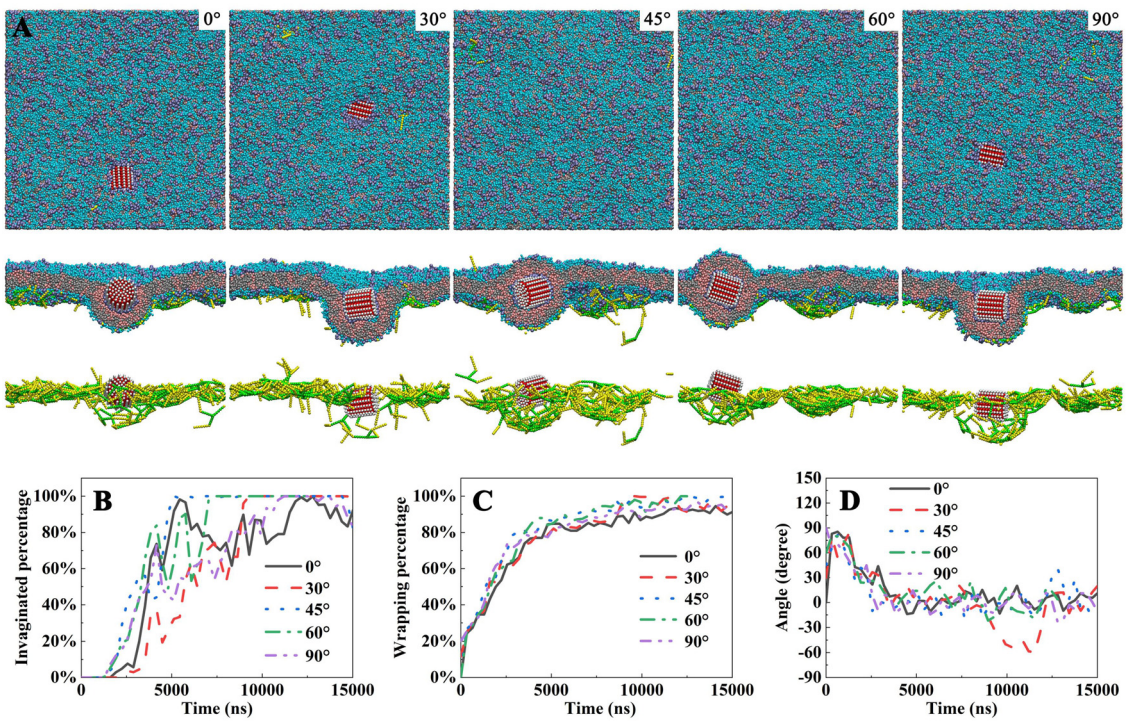

Fig. 3 Clathrin-mediated endocytosis for short rod-shaped NP (D = 5.8 nm and H = 5.8 nm) with different initial angles. (A) Final snapshots of membrane wrapping on different initial angles of short rod-shaped NPs from top, cross-sectional views, and only clathrin and NP. (B) Percentage of invagination as a function of time. (C) Percentage of wrapping as a function of time. (D) Evolution of short rod-shaped NP orientation angles. In the figure, five initial orientations were compared.

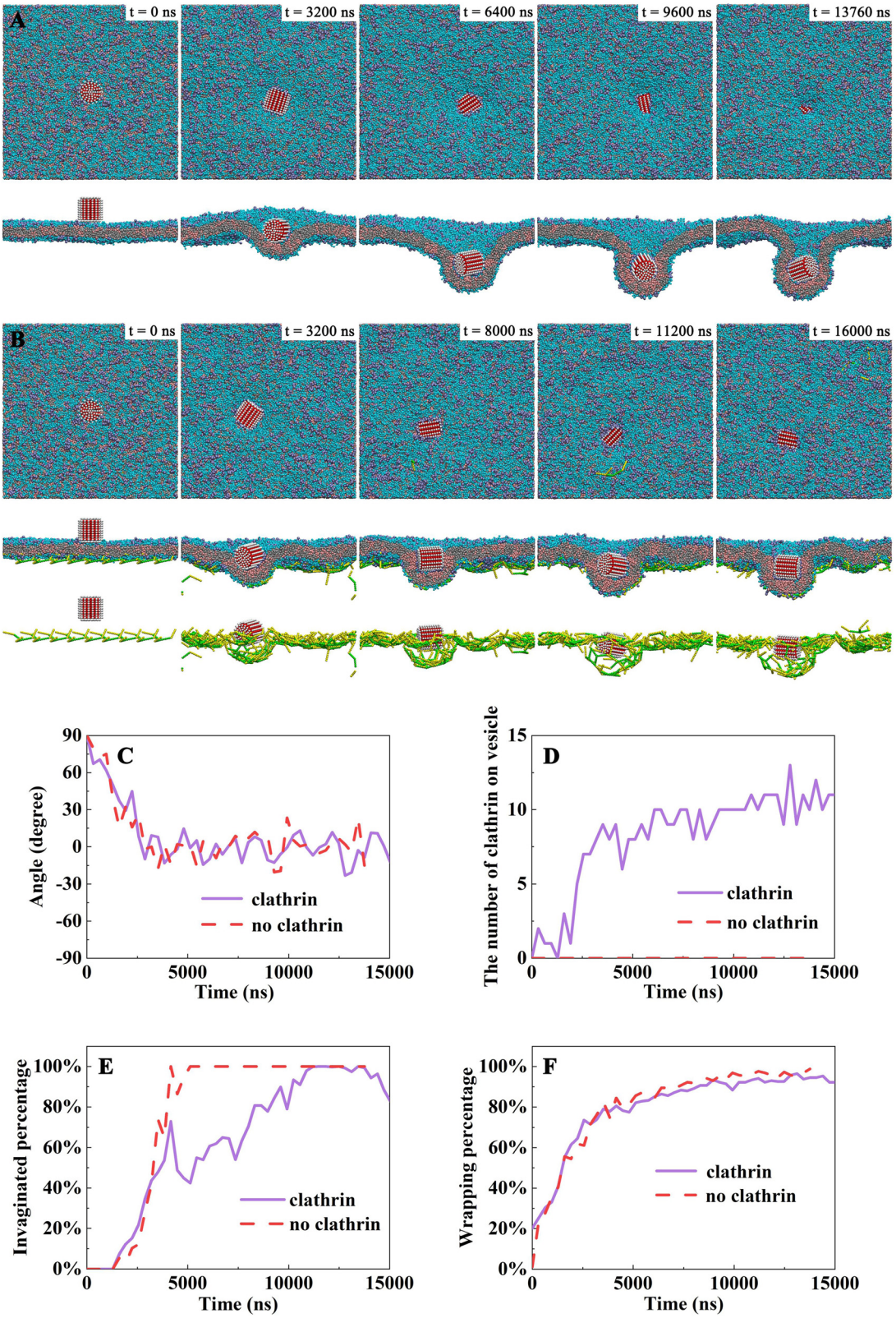

Fig. 4 Endocytosis kinetics for short rod-shaped NP with the initial orientation angle of 90°. Several typical snapshots during endocytosis of short rod-shaped NP in the absence of clathrin (A) and in the presence of clathrin (B). (C) Time evolutions of NP orientation angles. (D) Time evolutions of the clathrin number on vesicles. (E) Invaginated percentage of NPs as a function of time. (F) Wrapping percentage of NPs as a function of time.

In order to study the role of clathrins, we also compared the endocytosis process of short rod-shaped NPs in the absence (Fig. 4A) and presence of clathrins (Fig. 4B). The rotation of asymmetric NPs is always observed in the invagination stage (Fig. 4C). Similar to long rod-shaped NPs, the clathrin elongates during the invagination process for short rod-shaped NPs (Fig. 4E). However, in the wrapping stage, during the self-assembly of clathrins on the endocytic site (Fig. 4D), the wrapping of NP is facilitated by the clathrin-mediated cage (Fig. 4B and F).

3.1.3. Clathrin-mediated endocytosis of disk-shaped NPs. We also studied the endocytosis kinetics for the disk-shaped NP. The typical final snapshots of the CME at different initial angles of disk-shaped NPs are shown in Fig. 5A. Different from the receptor-mediated endocytosis,[20] the disk-shaped NP with an initial angle of 90° did not show the fastest invagination in CME (Fig. 5B). However, the NP with a tile angle is easier to be invaginated. For example, the disk-shaped NP with an initial angle of 60° showed the fast invagination. This is because the initial adhesion of clathrins increased the stiffness of the membrane, which is not beneficial for the invagination of disk-shaped NPs with an initial angle of 90°. However, for NPs with an initial tile angle, the rotation of NP can trigger clathrin rearrangement, which can promote the subsidence of NP. The cooperative relationship between the clathrin self-assembly and NP subsidence is very important for the internalization efficiency of shape asymmetric NPs. Only the effective clathrin-mediated cage formation at the endocytosis site can promote the subsidence and wrapping of NPs.

Rotation is also an obvious feature for disk-shaped NPs during CME. Usually, the rotation occurs twice for the successful endocytosis of disk-shaped NPs. In the invagination stage, due to the strong ligand–receptor binding energy, all different initial orientations of disk-shaped NPs rotate to about 75° (Fig. 5D). However, in the wrapping stage, disk-shaped NPs undergo the second rotation (Fig. 5D). Both the rotations in the invagination and wrapping stages are time-consuming (Fig. 5B–D). We found an interesting phenomenon that the disk-shaped NP with an initial angle of 0° rotated first in the wrapping stage, but not the disk-shaped NP with an initial angle of 90°. The disk-shaped NP with an initial angle of 90° has the largest contact area with the membrane, which is beneficial for ligand–receptor binding. From the evolution of disk-shaped NP orientation angles (Fig. 5D), we speculated that both the strong ligand–receptor binding energy and the local membrane rigidified by clathrin adhesion make the disk-shaped NP (ϕ_0 = 90°) get struck in a metastable equilibrium. How to break the metastable equilibrium and induce the further rotation of disk-shaped NPs (ϕ_0 = 90°) play a crucial role in its further wrapping. In order to investigate the trigger mechanism for the further rotation of NPs, we showed the details of the self-assembly of clathrins during the second rotation of disk-shaped NPs (ϕ_0 = 90°) in Fig. S2 (ESI†). Clathrin proteins assemble at the endocytic site, which can tiger NP rotation

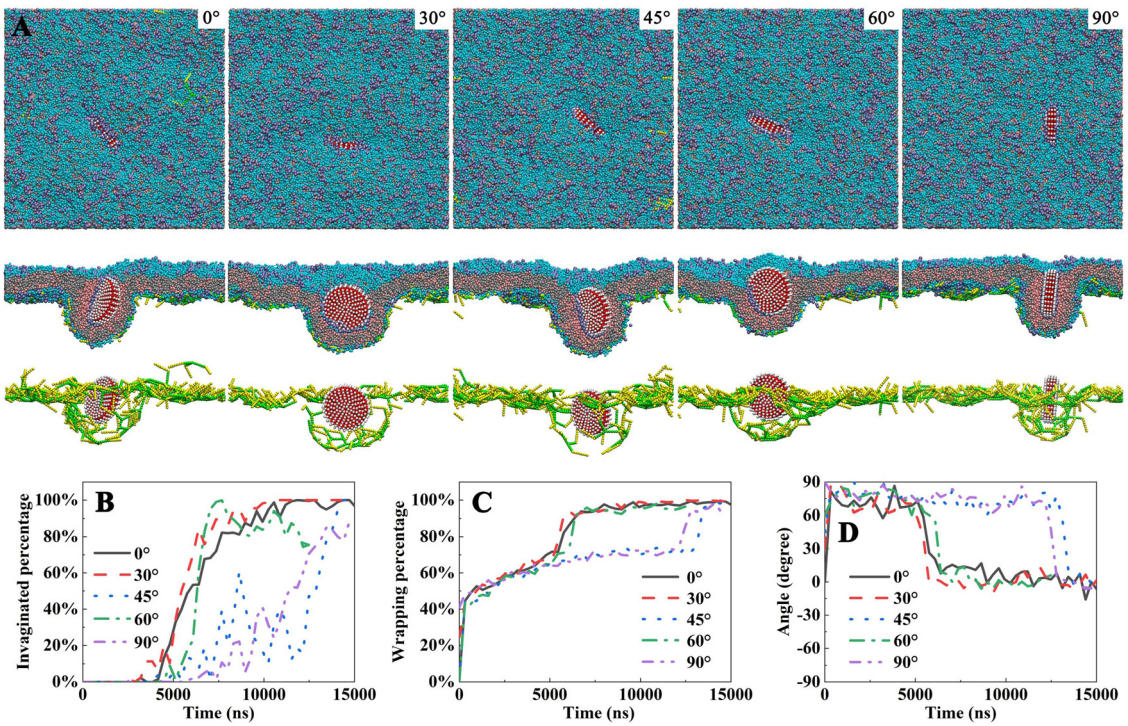

Fig. 5 Clathrin-mediated endocytosis for disk-shaped NP (D = 9.7 nm and H = 1.9 nm) with different initial angles. (A) Final snapshots of membrane wrapping on different initial angles of disk-shaped NPs from top, cross-sectional views, and only clathrin and NP. (B) Percentage of invagination as a function of time. (C) Percentage of wrapping as a function of time. (D) Evolution of disk-shaped NP orientation angle. In the figure, five initial orientations were compared.

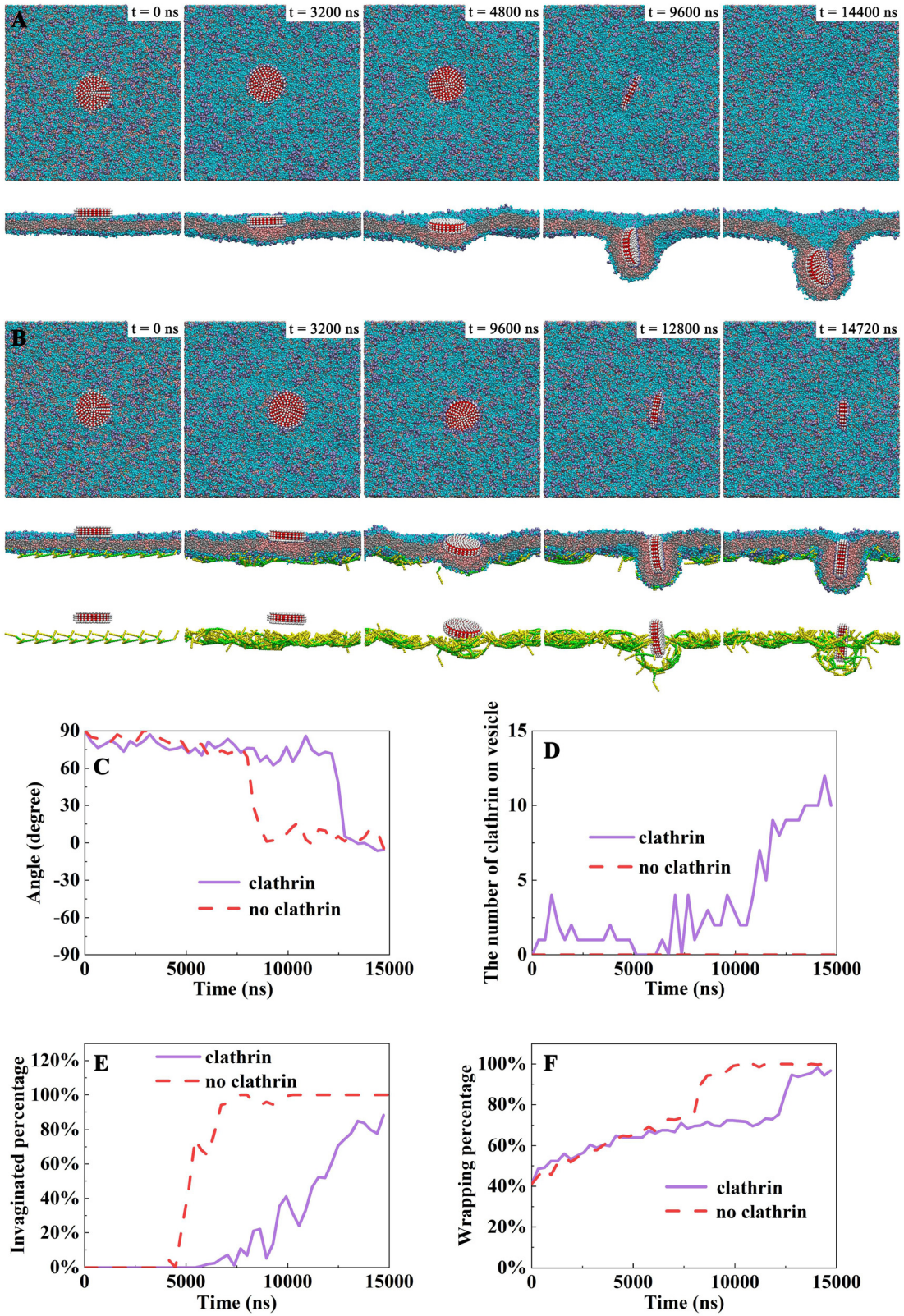

Fig. 6 Endocytosis kinetics for disk-shaped NP with the initial orientation angle of 90°. Several typical snapshots during endocytosis of disk-shaped NP in the absence of clathrin (A) and in the presence of clathrin (B). (C) Time evolutions of NP orientation angles. (D) Time evolutions of the clathrin number on vesicles. (E) Invaginated percentage of NPs as a function of time. (F) Wrapping percentage of NPs as a function of time.

(t = 12 160 ns) and promote NP wrapping (Fig. S2, ESI†). Finally, disk-shaped NP lying down on the membrane rotate itself and then become upright (t = 12 800 ns), which promotes receptor–ligand binding and membrane wrapping (Fig. S2, ESI†). The endocytosis can be failed without NP rotation. For example, one of the parallel simulation results shows that the disk-shaped NP with an initial angle of 30° finally did not become completely wrapped by the membrane (Fig. S3, ESI†), which was due to its delayed second rotation. However, this phenomenon may occur randomly, which is not because of the initial angle of the NP. In the finally wrapping stage, in order to finish the totally wrapping of NPs, the membrane need to bend further and promote the closure of the vesicle neck. Compared with the final engulfment process on receptor-mediated endocytosis, we found that the final engulfment process of NPs can be slightly different from clathrin-mediated endocytosis. In the presence of clathrins, it seems to elongate the closure of the vesicle neck, which is dependent upon the NP shape. The closure of the vesicle neck for disk-shaped NPs is more difficult in the presence of clathrins (Fig. 5A).

To further analyse the underlying molecular mechanism of CME, we compared the endocytosis of disk-shaped NPs (ϕ_0 = 90°) in the absence and presence of clathrins in Fig. 6A and B. It was found that the disk-shaped NP was completely sunk by a pure membrane in 7500 ns without clathrins, but a long relaxation time is required for disk-shaped NP invagination with clathrins (Fig. 6E), which further confirmed our conclusion that the stiffness of the membrane would enhance

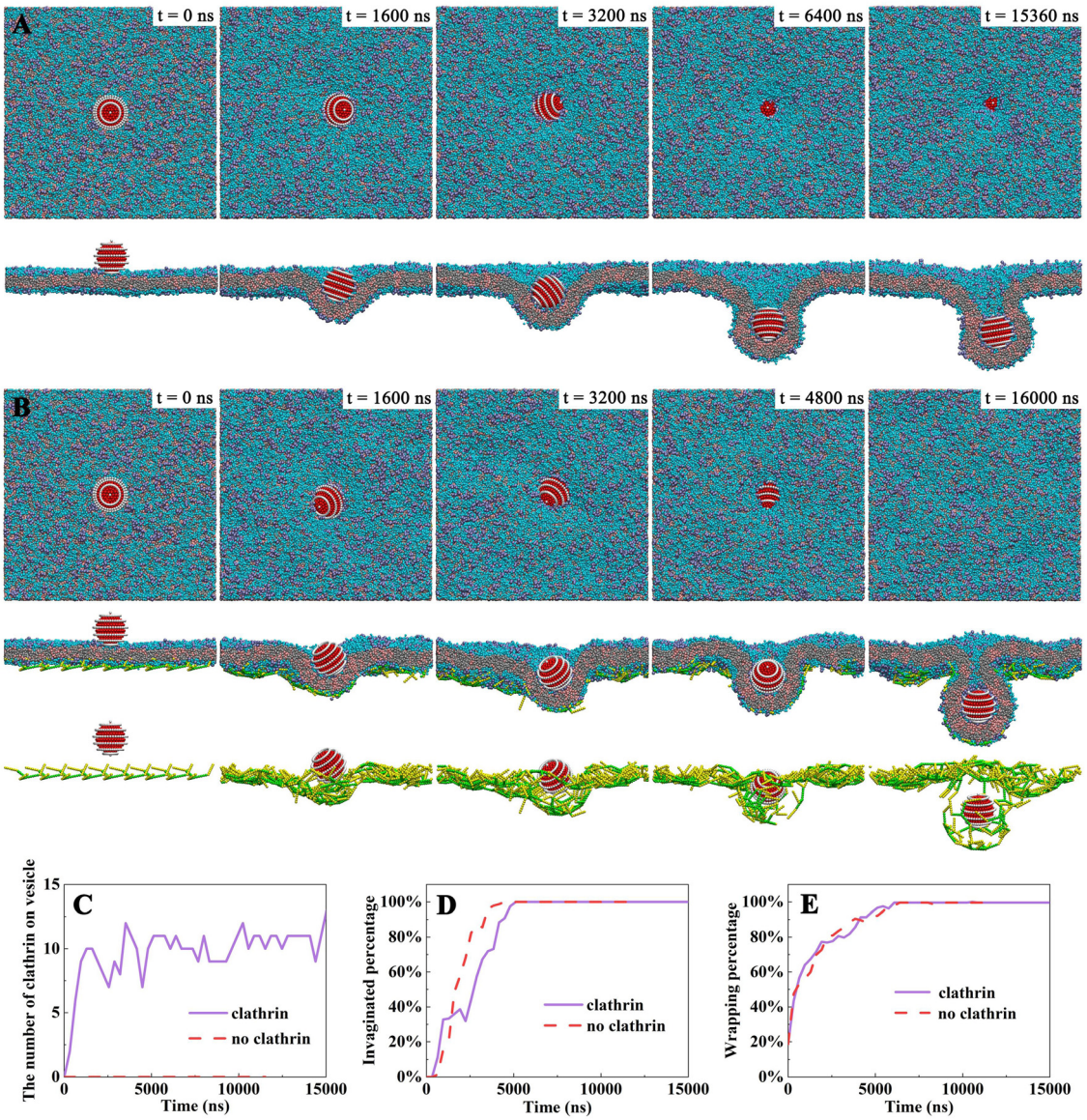

Fig. 7 Endocytosis kinetics for sphere-shaped NP (D = 7.1 nm). Several typical snapshots during endocytosis of sphere-shaped NP in the absence of clathrin (A) and in the presence of clathrin (B). (C) Time evolutions of the clathrin number on vesicles. (D) Invaginated percentage of NPs as a function of time. (E) Wrapping percentage of NPs as a function of time.

due to the initial adhesion of clathrins, which is not beneficial for direct NP invagination. During the wrapping process, more clathrin molecules accumulated at the endocytic site (Fig. 6B and D). The self-assembly of clathrins can trigger NP rotation (Fig. 6C). Finally, with the self-assembly of clathrins and NP rotation, the disk-shaped NP was completely wrapped by the membrane (Fig. 6B), but the wrapping process is still slower than that in the absence of clathrins (Fig. 6F).

3.1.4. Clathrin-mediated endocytosis of spherical NPs. To eliminate the shape anisotropy of NPs, we established a spherical NP as a control. The endocytosis of spherical NP without (Fig. 7A) and with clathrins (Fig. 7B) was considered. Similar to the other shaped NPs, the self-assembly of clathrins increased the hardness of the local patch membrane, which is not beneficial for NP invagination (Fig. 7D). However, in the wrapping stage, different from shape anisotropy NPs, the clathrin assembly on the surface of the membrane promoted membrane bending (Fig. 7C) and assisted membrane wrapping on spherical NPs (Fig. 7B and E), further confirming that the shape match or mismatch between the clathrin-mediated membrane vesicle and the shape of NP determines membrane wrapping on NPs is promoted or suppressed.

3.2. Dynamics wrapping mechanism for different shaped NPs with the clathrin self-assembly

3.2.1. Effect of NP shape. To compare the kinetics of CME of NPs with various shapes, as shown in Fig. 8, the rapidest invagination kinetics for different shaped NPs was chosen, such as the long rod-shaped NP and short rod-shaped NP with an initial orientation of 45°, and the disk-shaped NP with an initial orientation of 60°. The final snapshots of membrane wrapping on different shaped NPs in the presence of clathrins were shown in Fig. 8A. It should be noted that the kinetic behaviors for four different shapes of NPs were quite different, although they were wrapped by the membrane. In both the invagination and wrapping stages, the spherical NP exhibit the fast invagination and wrapping rate compared with other shaped NPs, and then are the short rod-shaped NP and the long rod-shaped NP (Fig. 8B and C). The disk-shaped NP showed the slowest invagination and wrapping rate (Fig. 8B and C). The number of clathrins on the vesicle with the endocytosis of different shaped NPs is shown in Fig. 8D.

3.2.2. Role of clathrins. To further compare the kinetic mechanism for different shaped NPs by CME, we discussed the

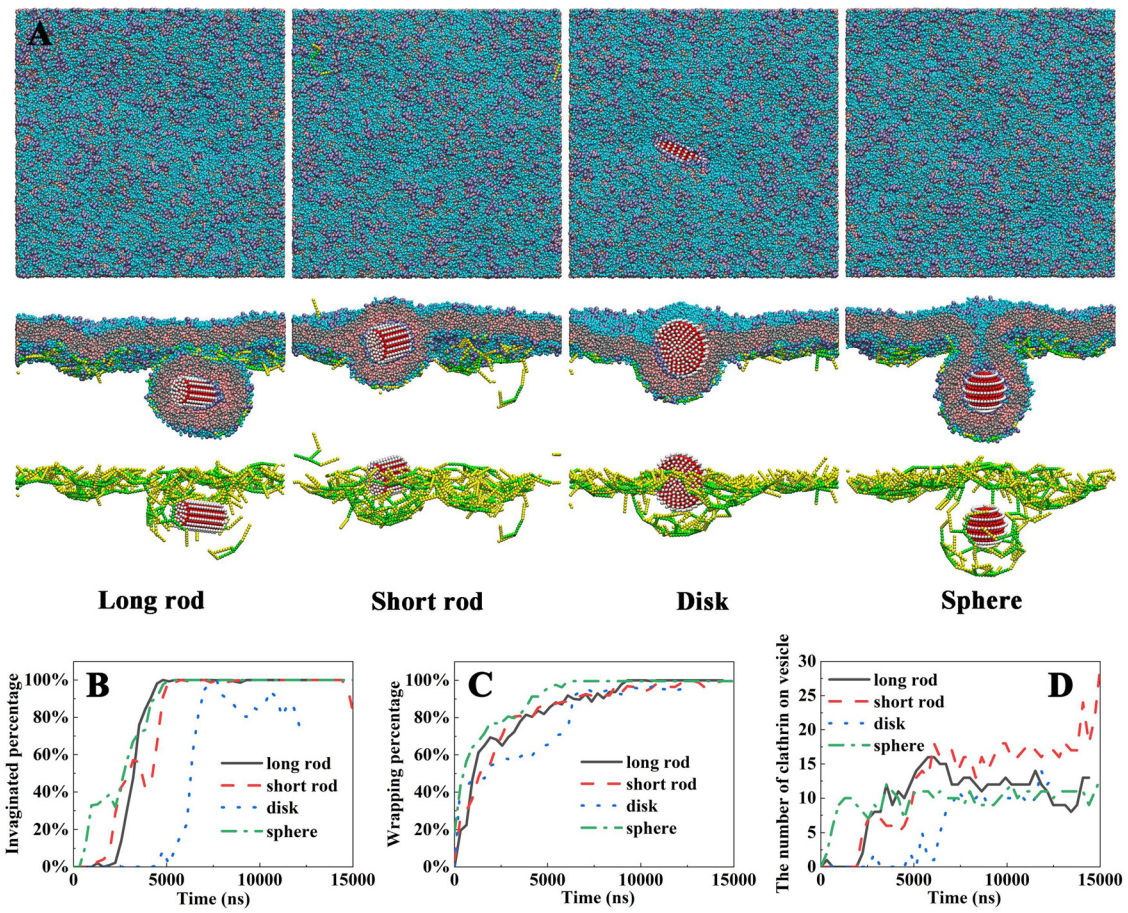

Fig. 8 Clathrin-mediated endocytosis for various shapes of NPs. In the figure, long rod-shaped NP adapt an initial angle 45°, short rod-shaped NP adapt an initial angle 45°, disk-shaped NP adapt an initial angle 60°. (A) Final snapshots of membrane wrapping on different shapes of NPs from top, cross-sectional views, and only clathrin and NP. (B) Invaginated percentage of NPs as a function of time. (C) Wrapping percentage of NPs as a function of time. (D) Time evolutions of NP orientation angles.

effect of clathrins in NP endocytosis. We found that the effect of clathrins for the endocytosis of different shapes of NPs is dependent upon the endocytosis stages. In the invagination stage, the clathrin initial adhesion would rigidify the local membrane patch, which is not beneficial for NP invagination and the influence for different shapes of NPs is similar. Compared with the condition without clathrins, the clathrin elongates during the subsidence process of NPs (Fig. 2E, 4E and 6E). In previous work, it has also been reported that the initial stage of endocytosis and the maximum invagination would be affected by clathrin coat,[19] which is consistent with our simulation results. However, in the wrapping stage, with the further self-assembly of clathrins on the endocytic site, clathrins can mediate different membrane responses for different shaped NPs during NP wrapping. Compared the kinetic behaviors of different shaped NPs by CME, the spherical NP has the fastest endocytosis rate (Fig. 8C). Usually, a wrapping process required membrane bending, which is relative to the largest local mean curvature of the NP. The spherical NP is more favorable for wrapping by the membrane than the shape anisotropy of NPs with the same volume in the pure membrane. Besides, the self-assembly of clathrins on the membrane can usually induce spherical vesicles, which is shape matched with the wrapping of spherical NP. However, for shape anisotropic NPs, there was shape mismatch between the intrinsic curvature of clathrin-mediated cage and the wrapping vesicle of shape anisotropic NPs. For example, it needs to form long rod-shaped vesicles to wrap long rod-shaped NPs (Fig. 8A), which has shape mismatch with the instinct clathrin-mediated cage structure. To reduce this mismatch, it can induce the rotation of shape anisotropic NPs and clathrin rearrangement to accomplish NP wrapping, both of these processes are time-consuming. Therefore, clathrins can assist the endocytosis of spherical NPs with the suitable size (Fig. 7E). For shape anisotropic NPs, our results indicated that the endocytosis efficiency for short rod-shaped NPs with an intermediate aspect ratio is higher than that with low or high aspect ratios (Fig. 8C). Based on the above-mentioned results, it can be concluded that CME have selectivity for NP shape. The internalization process can be elongated with the increased NP shape anisotropy.

To further investigate the role of clathrins for the endocytosis of different shaped NPs, the final clathrin density distribution for the endocytosis of various shapes of NPs is shown in Fig. 9, and the number of clathrins on endocytosis vesicle as a function of time is shown in Fig. S4 (ESI†). We can see that there have more clathrin molecules on the long rod-shaped NP and short rod-shaped NP with an initial orientation of 45°, and the disk-shaped NP with an initial orientation of 60° (Fig. 9). We further confirm that the effective self-assembly of clathrins on the endocytic site is very important for NP wrapping. On the contrary, the random clathrin self-assembly on the other site of the membrane can increase the stiffness of the membrane, which is not beneficial for NP wrapping.

3.2.3. Rotation for the endocytosis of shape anisotropy of NPs. Rotation is one of the typical characteristics for shape

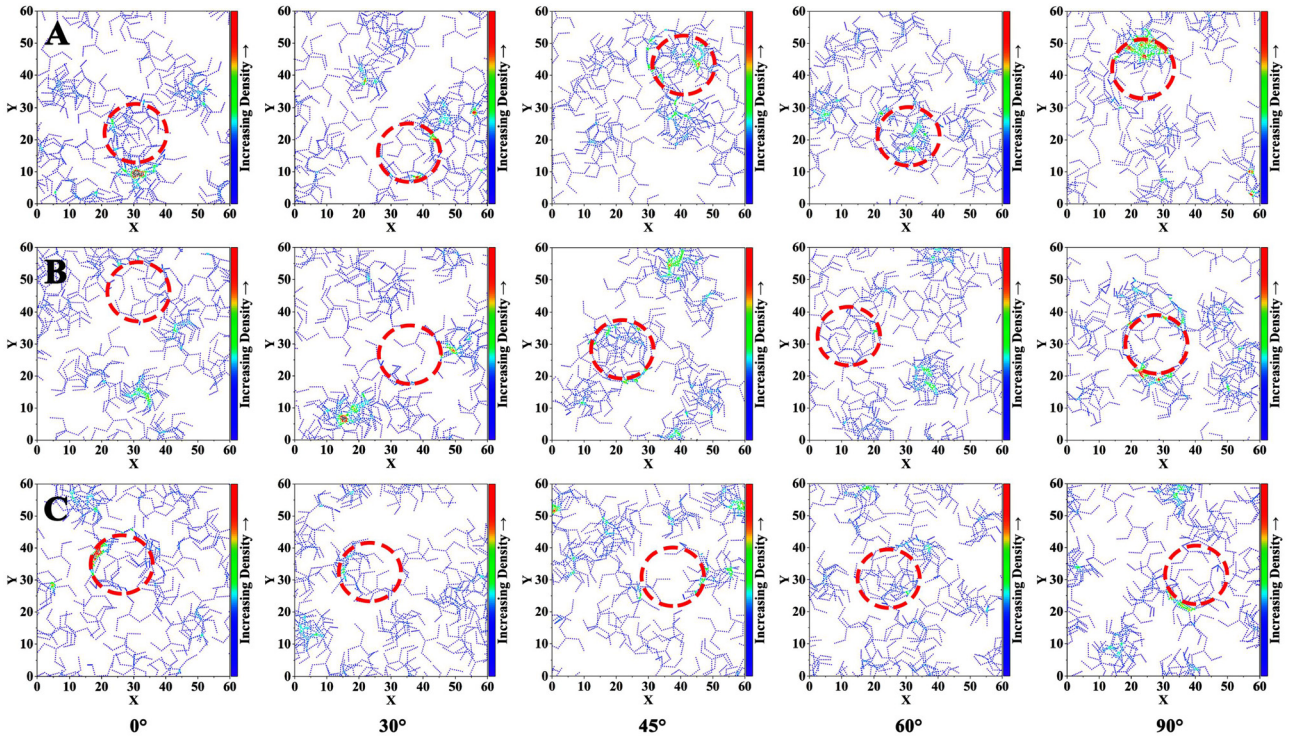

Fig. 9 The final clathrin density distribution for the endocytosis of various shaped NPs. (A) Clathrin-medisted endocytosis of long rod-shaped NP under corresponding conditions of Fig. 1A. (B) Clathrin-medisted endocytosis of short rod-shaped NP under corresponding conditions of Fig. 3A. (C) Clathrin-medisted endocytosis of disk-shaped NP under corresponding conditions of Fig. 5A. In the figure, five initial orientations of different shaped NPs were compared. From left to right, the initial orientations of NPs are 0°, 30°, 45°, 60°, 90°.

anisotropy of NPs by CME. The pathways predicated in Fig. 2B, 4B and 6B capture the general trend of endocytosis of shape anisotropy of NPs. In the invagination stage, different shaped NPs lay down the membrane with the large contact area. From a kinetics point of view, the ligand–receptor interaction provides the main driving force. However, the initial adhesion of clathrins on the membrane rigidified the local membrane patch. NPs with a tile angle can promote their subsidence. For example, the initial orientation of 60° of disk-shaped NPs showed the rapidest membrane invagination, but not the one with an initial orientation of 90° (Fig. 5B).

In the wrapping stage, with the increase in NP shape anisotropy, the rotation is also obvious in CME. For example, both of the long rod-shaped NP and disk-shaped NP rotate twice in CME (Fig. 1D and 5D). In the absence of clathrins, long rod-shaped NPs only show rotation in the invagination stage (Fig. 2A), but an obvious rotation is not found in the wrapping stage (Fig. 2A and C). On the one hand, the metastable equilibrium can be broken by the rotation of NPs, which promotes the subsidence of NPs and trigger the rearrangement of clathrins on the endocytic site. On the other hand, due to the shape mismatch between the instinct of the clathrin-mediated spherical vesicle and the wrapping of shape anisotropy NPs, the metastable equilibrium can mediate NP rotation to weaken the shape mismatch. Our results indicated that the rotation for shape anisotropy of NPs was more complex during CME, which is caused by the receptor–ligand binding, the self-assembly of clathrins, and membrane bending, and depends on the NP shape. Besides, the final orientation angle of NPs can be affected by the self-assembly of clathrins.

3.2.4. Effect of the NP size. In order to understand the effect of the NP size on CME, NPs of three different sizes with various shapes were designed: (1) Large-sized NPs, long rod-shaped NPs (D = 4.5 nm, L = 9.7 nm), short rod-shaped-NPs (D = 5.8 nm, L = 5.8 nm), disk-shaped NPs (D = 9.7 nm, L = 1.9 nm), and spherical NPs (D = 7.1 nm). (2) Middle-sized NPs, long rod-shaped NPs (D = 3.2 nm, L = 8.4 nm), short rod-shaped NPs (D = 4.5 nm, L = 4.5 nm), disk-shaped NPs (D = 7.1 nm, L = 1.9 nm), and spherical NPs (D = 4.5 nm). (3) Small-sized NPs, long rod-shaped NPs (D = 1.9 nm, L = 7.1 nm), short rod-shaped NPs (D = 3.2 nm, L = 3.2 nm), disk-shaped NPs (D = 4.5 nm, L = 1.3 nm), and spherical NPs (D = 3.2 nm). After simulation of 10 μs, compared the wrapping percentage of long rod-shaped NPs with different sizes, we found that the small long rod-shaped NP had the fastest wrapping ratio by CME than the other sizes of NPs with the same shape (Fig. S5A, ESI†). At the same time, the size effect for the wrapping of different shaped NPs has the same tendency (Fig. S5B–D, ESI†). In a real biological system, a clathrin leg is about 475 Å long.[71] In order to make the simulation in allowable spatial and temporal scales, we scaled down the size of clathrins and NPs. Our simulation results can qualitatively compared with the experimental

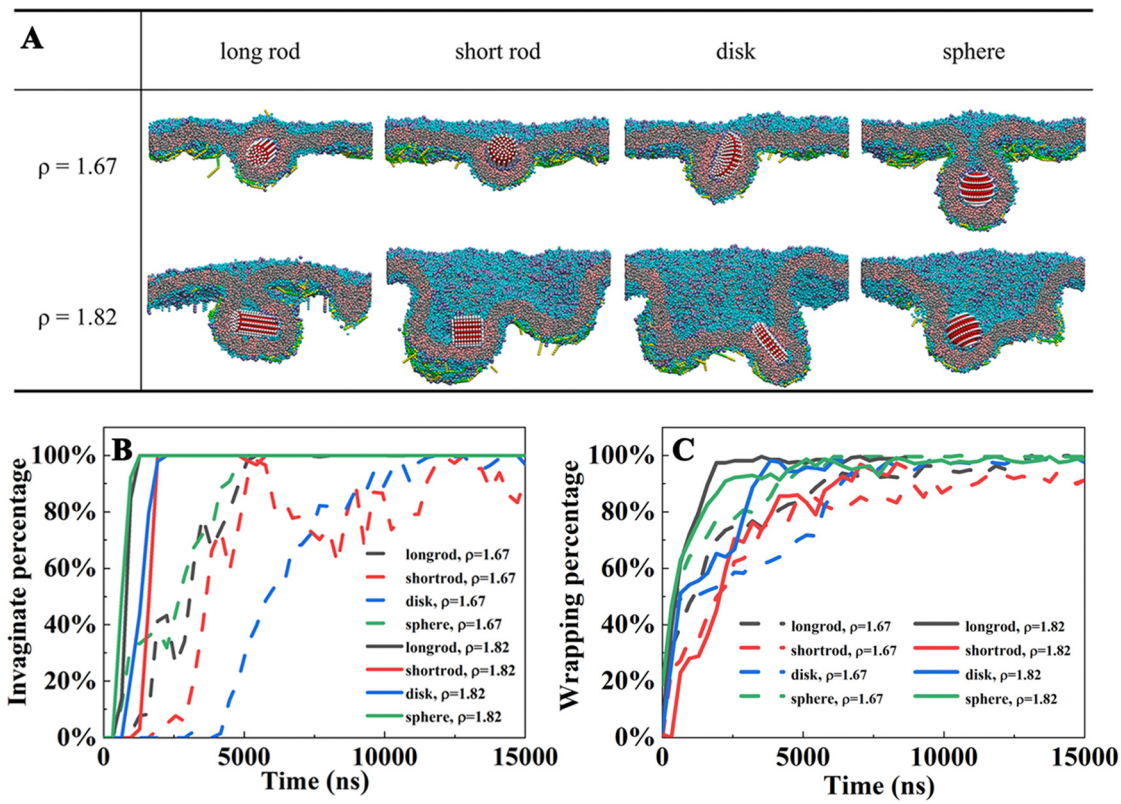

Fig. 10 Clathrin-mediated endocytosis for different shaped NPs with different membrane surface tensions. (A) Final snapshots for membrane wrapping on different shaped NPs. (B) Percentage of invagination as a function of time. (C) Percentage of wrapping as a function of time. The size of long rod-shaped NP (D = 4.5 nm, L = 9.7 nm), short rod-shaped NP (D = 5.8 nm, L = 5.8 nm), disk-shaped NP (D = 9.7 nm, L = 1.9 nm), spherical NP (D = 7.1 nm).

results. This is different from the endocytosis tendency in the absence of clathrins. Usually, the large NP is more favorable to be wrapped by a pure lipid membrane, which needs to overcome a smaller membrane bending energy. However, for CME, the size match or mismatch between the clathrin-mediated vesicle and the wrapping vesicle of NP determines whether the endocytosis of NP is promoted or inhibited.

3.2.5. Effect of membrane surface tension. In the practical cell, the cellular membrane may have different surface tensions. The surface tension of the membrane also plays a very important role in NP endocytosis. Therefore, in this work, we considered the effect of membrane surface tension and explored these cases for the different shaped NPs by CME, which are ρ_{LNPA}^{BR} = 1.67 to represent a small negative surface tension and ρ_{LNPA}^{BR} = 1.82 to represent a large negative surface tension. The final snapshots of membrane wrapping on different shaped NPs by CME are shown in Fig. 10A. It is found that the efficiency of NP invagination (Fig. 10B) and wrapping (Fig. 10C) is promoted by the decrease in membrane surface tension. Besides, the final structures shown in Fig. 10A reveal that when the surface tension of the membrane decreased, the self-assembly of clathrins on the membrane can mediate the occurrence of empty vesicles. At the same time, the final closure of the vesicle neck is elongated. The metastable state lasts for a long time. This is different from the case of absence of clathrins, our previous investigations indicated that asymmetric endocytosis can be induced by the shape anisotropy NP and the decrease in membrane tension.[22] However, the asymmetric endocytosis of shape anisotropy NPs was not found when the membrane tension was smaller in the presence of clathrins. On the contrary, the self-assembly of clathrins on the relaxed membrane can promote NP subsidence.

4. Conclusions

In summary, the dynamics mechanism for CME of different shaped NPs was investigated using DPD simulations. To gain a deep understanding of the coupling effect of the clathrin assembly and NP wrapping, four types of NPs were taken into account, namely, spherical NPs, long rod-shaped NPs, short rod-shaped NPs and disk-shaped NPs. Our simulations demonstrated that CME is sensitive to the NP shape. The spherical NP is more favorably wrapped by the membrane with the clathrin assembly. For rod-shaped NPs, NPs with the intermediate aspect ratios, such as the short rod-shaped NP, showed a higher endocytosis efficiency than that of NPs with low or high aspect ratios. In the process of CME, the effect of clathrins on the membrane is complex. In the invagination stage, the local membrane patch is rigidified by the clathrin coat, which is not beneficial for NP invagination. However, in the wrapping stage, it has been indicated that the self-assembly of clathrins promoted bending of the membrane, which can accelerate the wrapping of spherical NPs with the suitable size. However, for rod-shaped NPs, there is shape mismatch between the intrinsic curvature of the clathrin-mediated cage structure and the wrapping of anisotropic NPs. This mismatch can induce NP rotation in the wrapping stage, and clathrin rearrangement to accomplish NP wrapping. Both of these processes are time-consuming. In addition, the surface charge, stiffness, and the ligand of NPs are also very important for NP internalization, which will be investigated in our future work. In summary, our results help gain a deep understanding of the dynamics mechanism of CME of different shaped NPs, providing a guidance for the design of NPs with an optimal shape in the drug/gene delivery field.

Author contributions

Ye Li conceive the idea, perform the simulation and write-original manuscript; Man Zhang investigation and formal analysis; Yezhuo Zhang and Xinhui Niu software and visualization; Zhendan Liu and Wen Zhang visualization; Tongtao Yue review & editing.

Conflicts of interest

There are no conflicts of interest to declare.

Acknowledgements

This work is supported by ''the Fundamental Research Funds for the Central Universities'' (2021ZY56), the National Natural Science Foundation of China (31601149), the Municipal Training Program of Innovation and Entrepreneurship for Undergraduates, Beijing Forestry University, China (S202210022049), the National Key Research and Development Program of China (2022YFF0712500), the Program of Introducing Talents of Discipline to Universities (111 project, B13007). The authors thank ''Chem. Cloud Computing'' of BUCT.

References

1 K. Pefani-Antimisiari, D. K. Athanasopoulos, A. Marazioti, K. Sklias, M. Rodi, A.-L. De Lastic, A. Mouzaki, P. Svarnas and S. G. Antimisiaris, *Sci. Rep.*, 2021, **11**, 1–15.
2 H. Wu, Y. Hua, J. Wu, Q. Zeng, X. Yang, X. Zhu and X. Zhang, *Nano Res.*, 2022, **15**, 6256–6265.
3 H. Yuan, H. Y. Liang, P. D. Hou and J. Li, *Chem. Res. Chinese Univ.*, 2021, **37**, 840–845.
4 S. Z. M. Isa, R. Zainon and M. Tamal, *Materials*, 2022, **15**, 875.
5 J. C. Hsiao, T. Buryska, E. Kim, P. D. Howes and A. J. deMello, *Nanoscale*, 2021, **13**, 4956–4970.
6 N. Boehnke, J. P. Straehla, H. C. Safford, M. Kocak, M. G. Rees, M. Ronan, D. Rosenberg, C. H. Adelmann, R. R. Chivukula, N. Nabar, A. G. Berger, N. G. Lamson, J. H. Cheah, H. Li, J. A. Roth, A. N. Koehler and P. T. Hammond, *Science*, 2022, **377**, eabm5551.
7 W. S. Yun, J. H. Park, D. K. Lim, C. H. Ahn, I. C. Sun and K. Kim, *Cancers*, 2022, **14**, 2044.

8 Z. Hu, Y. Pan, J. Wang, J. Chen, J. Li and L. Ren, *Biomed. Pharmacother.*, 2009, **63**, 155–164.
9 H. J. Eom and J. Choi, *Chem. - Biol. Interact.*, 2019, **311**, 108774.
10 E. Huerta-García, M. D. P. Ramos-Godinez, A. López-Saavedra, E. Alfaro-Moreno, N. P. Gómez-Crisóstomo, Z. Colín-Val, H. Sánchez-Barrera and R. López-Marure, *Chem. Res. Toxicol.*, 2019, **32**, 578–588.
11 U. Singh, A. G. Teja, S. Walia, P. Vaswani, S. Dalvi and D. Bhatia, *Nanoscale Adv.*, 2022, **4**, 1375–1386.
12 Y. H. Feng, B. Z. Chen, W. M. Fei, Y. Cui, C. Y. Zhang and X. D. Guo, *AIChE J.*, 2022, **68**, e17507.
13 Y. Wei, H. Chen, Y. Li, K. He, K. Yang and H. Pang, *ACS Nano*, 2022, **16**, 5885–5897.
14 Y. Li, M. Zhang, X. Niu and T. Yue, *Colloids Surf., B*, 2022, **214**, 112467.
15 P. Hu, J. An, M. M. Faulkner, H. Wu, Z. Li, X. Tian and J. P. Giraldo, *ACS Nano*, 2020, **14**, 7970–7986.
16 G. Su, X. Zhou, H. Zhou, Y. Li, X. Zhang, Y. Liu, D. Cao and B. Yan, *ACS Appl. Mater. Interfaces*, 2016, **8**, 30037–30047.
17 S. Zhang, J. Li, G. Lykotrafitis, G. Bao and S. Suresh, *Adv. Mater.*, 2009, **21**, 419–424.
18 Y. S. Wei, H. B. Chen, Y. X. Li, K. J. He, K. Yang and H. B. Pang, *ACS Nano*, 2022, **16**, 5885–5897.
19 W. Xu, X. H. Liu and X. H. Liu, *J. Appl. Phys.*, 2022, **131**, 134701.
20 B. D. Chithrani and W. C. Chan, *Nano Lett.*, 2007, **7**, 1542–1550.
21 K. Xiong, J. Zhao, D. Yang, Q. Cheng, J. Wang and H. Ji, *Soft Matter*, 2017, **13**, 4644–4652.
22 Y. Li, T. Yue, K. Yang and X. Zhang, *Biomaterials*, 2012, **33**, 4965–4973.
23 R. Vácha, F. J. Martinez-Veracoechea and D. Frenkel, *Nano Lett.*, 2011, **11**, 5391–5395.
24 K. Yang and Y. Q. Ma, *Nat. Nanotechnol.*, 2010, **5**, 579–583.
25 T. Yue, X. Wang, F. Huang and X. Zhang, *Nanoscale*, 2013, **5**, 9888–9896.
26 J. Xu, L. Wen, F. Zhang, W. Lin and L. Zhang, *J. Colloid Interface Sci.*, 2021, **597**, 114–125.
27 Z. Shen, H. Ye, X. Yi and Y. Li, *ACS Nano*, 2019, **13**, 215–228.
28 X. Yi and H. Gao, *Phys. Rev. E*, 2014, **89**, 062712.
29 N. Liu, M. Becton, L. Zhang and X. Wang, *J. Phys. Chem. B*, 2020, **124**, 11145–11156.
30 Y. Li, X. Zhang and D. Cao, *Nanoscale*, 2015, **7**, 2758–2769.
31 A. Avellan, J. Yun, Y. Zhang, E. Spielman-Sun, J. M. Unrine, J. Thieme, J. Li, E. Lombi, G. Bland and G. V. Lowry, *ACS Nano*, 2019, **13**, 5291–5305.
32 A. Verma, O. Uzun, Y. Hu, Y. Hu, H.-S. Han, N. Watson, S. Chen, D. J. Irvine and F. Stellacci, *Nat. Mater.*, 2008, **7**, 588–595.
33 I. K. Mati, W. Edwards, D. Marson, E. J. Howe, S. Stinson, P. Posocco and E. R. Kay, *ACS Nano*, 2021, **15**, 8295–8305.
34 Y. Li, X. Zhang and D. Cao, *Soft Matter*, 2014, **10**, 6844–6856.
35 J. Rejman, V. Oberle, I. S. Zuhorn and D. Hoekstra, *Biochem. J.*, 2004, **377**, 159–169.
36 J. M. Oh, S. J. Choi, G. E. Lee, J. E. Kim and J. H. Choy, *Chem. – Asian J.*, 2009, **4**, 67–73.
37 O. Zimmer and A. Goepferich, *Nanoscale Horiz.*, 2023, **8**, 256–269.
38 H. Deng, P. Dutta and J. Liu, *Biochim. Biophys. Acta, Gen. Subj.*, 2018, **1862**, 2104–2111.
39 O. Harush-Frenkel, N. Debotton, S. Benita and Y. Altschuler, *Biochem. Biophys. Res. Commun.*, 2007, **353**, 26–32.
40 S. Zhou, J. Wu, X. Huang, N. Yu, X. Zou, H. Tang, J. Singh, B. Song and Y. Li, *Mater. Des.*, 2021, **200**, 109464.
41 A. Chakraborty and N. R. Jana, *J. Phys. Chem. Lett.*, 2015, **6**, 3688–3697.
42 S. Engelberg, J. Modrejewski, J. G. Walter, Y. D. Livney and Y. G. Assaraf, *Oncotarget*, 2018, **9**, 20993.
43 C. Zhu, X. Zhou, Z. Liu, H. Chen, H. Wu, X. Yang, X. Zhu, J. Ma and H. Dong, *Front. Mol. Biosci.*, 2021, **8**, 627015.
44 E. Allard-Vannier, K. Hervé-Aubert, K. Kaaki, T. Blondy, A. Shebanova, K. V. Shaitan, A. A. Ignatova, M. L. Saboungi, A. V. Feofanov and I. Chourpa, *Biochim. Biophys. Acta, Gen. Subj.*, 2017, **1861**, 1578–1586.
45 Z. Shen, H. Ye, X. Yi and Y. Li, *ACS Nano*, 2018, **13**, 215–228.
46 S. Zhang, H. Gao and G. Bao, *ACS Nano*, 2015, **9**, 8655–8671.
47 Y. Shao, L. Xiang, W. Zhang and Y. Chen, *J. Controlled Release*, 2022, **352**, 600–618.
48 H. Deng, P. Dutta and J. Liu, *Soft Matter*, 2019, **15**, 5128–5137.
49 K. Yang and Y.-Q. Ma, *Nat. Nanotechnol.*, 2010, **5**, 579–583.
50 H. Deng, P. Dutta and J. Liu, *Nanoscale*, 2019, **11**, 11227–11235.
51 C. Huang, Y. Zhang, H. Yuan, H. Gao and S. Zhang, *Nano Lett.*, 2013, **13**, 4546–4550.
52 L. Ou, H. Chen, B. Yuan and K. Yang, *ACS Nano*, 2022, **16**, 18090–18100.
53 M. Venturoli, M. Maddalena Sperotto, M. Kranenburg and B. Smit, *Phys. Rep.*, 2006, **437**, 1–54.
54 M. Kranenburg and B. Smit, *J. Phys. Chem. B*, 2005, **109**, 6553–6563.
55 E. M. Schmid and H. T. McMahon, *Nature*, 2007, **448**, 883–888.
56 M. P. Czech, *Cell*, 2000, **100**, 603–606.
57 A. Fotin, Y. Cheng, P. Sliz, N. Grigorieff, S. C. Harrison, T. Kirchhausen and T. Walz, *Nature*, 2004, **432**, 573–579.
58 J. Mao, R. Guo and L. T. Yan, *Biomaterials*, 2014, **35**, 6069–6077.
59 X. Lin, X. Lin and N. Gu, *Nanoscale*, 2020, **12**, 4101–4109.
60 Y. Li, X. Li, Z. Li and H. Gao, *Nanoscale*, 2012, **4**, 3768–3775.
61 P. Chen, H. Yue, X. Zhai, Z. Huang, G. H. Ma, W. Wei and L. T. Yan, *Sci. Adv.*, 2019, **5**, eaaw3192.
62 Y. Li, X. Zhang, J. Lin, R. Li and T. Yue, *Colloids Surf., B*, 2019, **176**, 239–248.
63 S. Ma, Y. Hu and R. Wang, *Macromolecules*, 2015, **48**, 3112–3120.
64 R. D. Groot and T. J. Madden, *J. Chem. Phys.*, 1998, **108**, 8713–8724.
65 J. C. Shillcock and R. Lipowsky, *J. Chem. Phys.*, 2002, **117**, 5048–5061.
66 R. D. Groot and P. B. Warren, *J. Chem. Phys.*, 1997, **107**, 4423–4435.

67 T. Yue and X. Zhang, *Soft Matter*, 2011, **7**, 9104–9112.
68 Y. Li, T. Yue, K. Yang and X. Zhang, *Biomaterials*, 2012, **33**, 4965–4973.
69 L. Huang, D. Chen, Y. Ding, S. Feng, Z. L. Wang and M. Liu, *Nano Lett.*, 2013, **13**, 3135–3139.
70 R. Vácha, F. J. Martinez-Veracoechea and D. Frenkel, *Nano Lett.*, 2011, **11**, 5391–5395.
71 V. A. Zborowski, M. H. Sari, S. O. Heck, E. C. Stangherlin, J. S. Neto, C. W. Nogueira and G. Zeni, *Physiol. Behav.*, 2016, **164**, 25–33.